Flexible integrated sensing platform for monitoring wound temperature and predicting infection

Yuheng Zhang,[1,†] Bin Lin,[1,†] Rong Huang,[1,†] Zhixiao Lin,[1] Yongqian Li,[2] Jinqing Li[1**] and Xueyong Li[1*] (iD)

[1]Department of Burn and Plastic Surgery, Second Affiliated Hospital of Air Force Military Medical University, Xi'an, 710000, China.
[2]Key Laboratory of Micro/Nano Systems for Aerospace of the Ministry of Education, Northwestern Polytechnical University, Xi'an, Shaanxi, 710072, China.

Summary

Wound infection is a challenging clinical problem that imposes substantial economic and psychological burdens on patients. However, the wound covered by a dressing is in an 'unknown' state. Recently, researchers have focused on understanding the condition of the wound without removing the dressing. Here, we presented a flexible integrated sensing platform (FISP) that can monitor multiple indicators, including local temperature. The platform consists of a flexible sensor chip (FSC), a controlled printed circuit board (CPCB) and a customized application installed on a smartphone that can receive and display data from the sensor chip through Bluetooth Low Energy 4.0 (BLE4.0) and upload real-time wound information. This device exhibits satisfactory measurement accuracy, stability, durability, skin compliance and biocompatibility. It was applied to infected wounds on the back of rabbits to reveal the temperature changes characteristic of wounds infected with different bacteria, and this information was compared with the changes in the core body temperature of animals. We found differences in the temperature among wounds infected with different pathogens and the temperature of the wound infection occurred earlier than the change in anal temperature. The combined application of the FISP and dressings might help identify the 'unknown' state of wounds in the clinic.

Introduction

With the development of an ageing society, chronic diseases, such as senile diseases, metabolic diseases and vascular diseases, are increasing annually; in addition, a high incidence of chronic wounds, such as diabetic foot, pressure sores, venous ulcers of the lower limbs and cancerous ulcers, are also noted in elderly populations (Nicholas *et al.*, 2013; Frykberg and Banks, 2015; Powers *et al.*, 2016). Approximately 1.5–2.0 million patients in Europe and 2.4–4.5 million patients in the United States suffer from non-healing wounds caused by diabetes, hypertension, hyperuricaemia and venous ulcers, and the treatment costs associated with these populations account for approximately 2–3% of total healthcare expenditures (Frykberg and Banks, 2015; Lindholm and Searle, 2016; Ruth *et al.*, 2018). Chronic wounds are all complicated with different degrees of infection, and their treatment has become a major challenge in both developed and developing countries (Phillips *et al.*, 2016). The social and economic burden caused by chronically infected wounds is underappreciated and growing; however, efforts devoted to the treatment of this type of wound have yielded minimal satisfying achievements (Sen *et al.*, 2009; Olsson *et al.*, 2019). To date, the most commonly used method to treat wounds is a dressing change, but when and whether the dressing should be changed has not been standardized. One indication for a dressing change is when the dressing is permeated by exudate, but the dressing change is obviously too late when this sign is observed. The wound state should be used to guide the dressing change, but this information can only be obtained by opening the dressing to observe the current state of the wound. This traditional wound evaluation method lacks an objective basis and relies mainly on the level and clinical experience of the attending physician. On the other hand, repeated dressing changes would not only interfere with the normal wound healing process but also impose great physical and mental pain on patients, increase the work load of medical staff, waste medical resources, and increase the socio-economic burden(Collier and Hollinworth, 2000; Powers *et al.*, 2016). Most of the active ingredients used in debridement, such as hydrogen peroxide and ionic silver preparations, are locally toxic and exhibit limited or no proven efficacy in enhancing wound healing (Robert and Martin, 2012). More importantly, repeated exposure

and excessive medical intervention themselves are factors that might increase the risk of wound infection. In particular, in sudden situations when a serious shortage of medical resources emerges, such as wars and natural disasters, medical staff are unable to easily change dressings in a timely manner, which may delay treatment and lead to wound deterioration. Moreover, the evaluation of wound healing should occur throughout the treatment process, but traditional treatment methods based on clinical experience are obviously unable to meet this demand (Marieke, 2018). Therefore, the development of a new wound management method that monitors healing in real time is urgently needed.

Given the sustained progress in understanding wound healing, the potential relationships between the wound microenvironment and clinical outcome have been widely recognized (Junker *et al.*, 2013). The wound microenvironment refers to physical or chemical factors outside and adjacent to the wound that may be related to the clinical outcome of the wound (Kruse *et al.*, 2015). Among them, the local temperature of wounds is often considered a predictor of infection (Tegl *et al.*, 2015; Power *et al.*, 2017). When the temperature of a wound is < 33°C, wound repair is hindered (Kurz *et al.*, 1996; McGuiness *et al.*, 2004). The local temperature of acute wounds may be > 37°C due to local congestion and inflammation; on the other hand, a sudden increase in wound temperature is regarded as a sign of infection (Fierheller and Sibbald, 2010). Although local temperature is an important indicator of the wound state, few suitable methods are available to monitor it in real time during wound healing. The traditional mercury thermometer has difficulty fitting in the wound, and it takes a long time to calibrate. Thus, this device is obviously not suitable for clinical application. Given the wrapping of layers of dressings, the infrared thermometer is not suitable. With the intelligence and miniaturization of sensors, biological dressings can realize real-time monitoring of the wound microenvironment combined with flexible substrate integrated circuit and wireless communication technology, which might provide medical staff with wound data to assess the healing state (Payam et al., 2017). Matzeu et al. developed a wireless sensor for monitoring skin temperature, which is mainly composed of a thermistor and radio frequency identification technology and has been applied in dressings or bandages (Matzeu *et al.*, 2016). Pang *et al.* (2020) designed a double-layer smart flexible electronics-integrated wound dressing by combining flexible electronic components with an antibacterial hydrogel to monitor the wound temperature in real time and release antibiotics from the hydrogel upon in situ UV irradiation. This series of studies shows the feasibility of monitoring the wound microenvironment using sensors.

Here, we report a flexible integrated sensing platform (FISP) that includes a flexible sensor chip (FSC), a controlled printed circuit board (CPCB) and a customized application installed on a smartphone. The FISP monitored the local temperature of wounds and was used as an early predictor of pathological infection. In addition, we established wounds infected with different bacteria, and the temperatures of these wounds were continuously monitored using the platform. The data were transmitted to smartphones via Bluetooth Low Energy (BLE) to reveal the changes in temperature of the wounds infected with different strains. The establishment of FISP is expected to realize the continuous monitoring of the wound healing process, overcome the 'unknown' state of wounds under dressings, and provide some assistance with clinical wound diagnosis and treatment.

Results

Structure and work scenario of the FISP

Figure 1A shows the diagram of FISP application under ideal conditions. The FISP would be fixed in a wound that is routinely bandaged with gauze, and the perceived data were sent to the smartphone for display through BLE to realize the real-time monitoring of the state of the wound. The FISP was engineered as a separate structure of flexible and hard plates to ensure that it would be able to adapt to wounds with different positions, shapes and depths (Fig. 1Bb). The FSC was the core of the whole integrated sensing module on which the sensing elements were welded, including temperature and humidity sensors and other components. With moderate flexibility and strong strength, PI was selected as the material for generating flexible substrates, where the elements were connected with serpentine copper film interconnects (Fig. 1Ba). The control platform outside the dressings adopted the conventional CPCB to coordinate the work of each part and process data, including the BLE antenna, signal amplifier, analogue-to-digital converter, digital controller and power interface (Fig. 1Bc). The FSC was connected to the CPCB by FFC, and the joint was smeared with an appropriate amount of silica gel to protect the welding interface and prevent excess activity. Fig. 1Bd and Be presents a figure of the device described above and the details of the electronic circuits. In addition, a special mobile phone app was developed to receive, display, store and upload multiple groups of data after processing at the same time to monitor wound healing. The FISP has the potential to play a significant role in telemedicine, AI diagnosis and precision medicine. In peacetime, it could be useful in community medical care and provide convenience by facilitating doctors' remote guidance. In public health events, it could be used for centralized monitoring of wounds in hospitalized
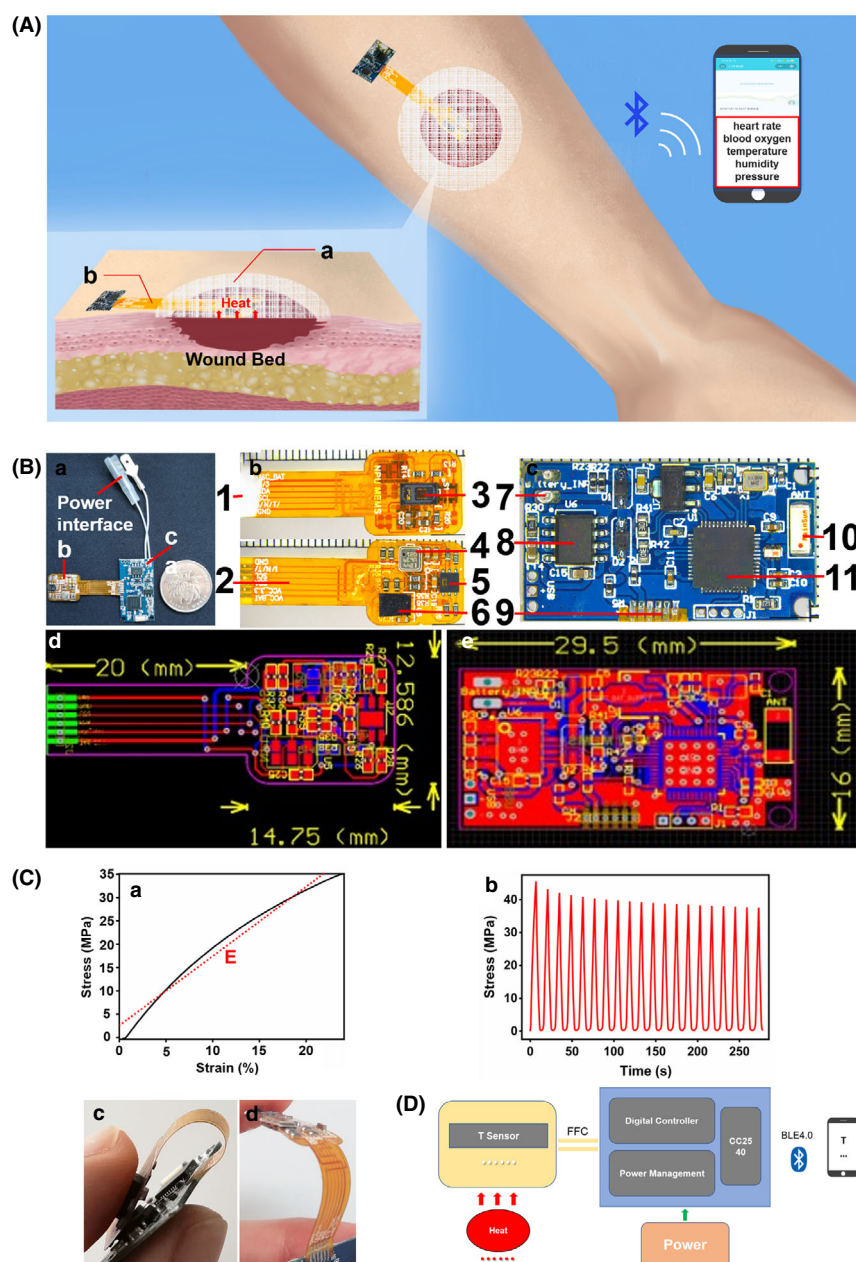
Fig. 1. Structures, application scenario and mechanical properties of the FISP.
A. The FISP is applied to the wound. The temperature of the wound is detected using a temperature sensor. Signals are processed by the hardware system, wirelessly sent to a smartphone by BLE and displayed in an app. The red arrows indicate the direction of heat transfer in the wound bed. (a. gauze and b. FISP) B. Gross and ultra-micro view of the FISP (a), which includes the FSC (b) and CPCB (c). Various sensors and electronic components are welded on these devices. The details of the electronic circuits are shown below (d–e). (1. silica gel, 2. FFC, 3. heart rate and blood oxygen saturation sensor, 4. pressure sensor, 5. temperature and humidity sensor, 6. pH-sensitive membrane, 7. power interface, 8. power management, 9. FFC soldering point, 10. BLE antenna and 11. digital controller) C. a. Stretchability of the flexible substrate. The stress–strain curve reveals the maximum tensile ratio. Young's modulus was calculated from the regression line (red dotted line). b. Mechanical reliability of the flexible substrate in a cyclic stress test. The time–stress curve depicts stretching at 7% for 20 cycles. c-d. Image of a curved FSC, which was restored after reaching the maximum bend.
D. System-level block diagram of the wound dressing system.

patients to save scarce medical resources and reduce unnecessary contact between doctors and patients when infectious diseases such as COVID-19 occur as well (Fig. S1).

Characteristics, reliability and biocompatibility of the FSC

The FSC exhibited multi-angle bending deformation, enabling it to work normally in several types of possible

complex situations during use (Fig. 1Da and Db). The mechanical properties of the integrated system were evaluated using a tensile test. The maximum tensile ratio of FSC was approximately 25% (Fig. 1Dc), and Young's modulus was also obtained from the stress–strain curve (Fig. 1Dc, red dotted line), which should be sufficient to satisfy routine skin deformation and movement within normal use. The device exhibited Young's modulus of approximately 25 MPa and good fatigue resistance when stretched at a maximum strain of 7% for 20 cycles (Fig. 1Dd), indicating that the system had the ability to work continuously.

After powering on the device and Bluetooth on the smart phone, the device was found on the app interface. After clicking, sensor information was received (Fig. 2Aa–d). The local temperature and humidity of the wounds, pressure, heart rate and blood oxygen saturation were monitored (Fig. 2Ad). Satisfactory measurement accuracy and stability are the prerequisites for sensors to accurately reflect the state of the wound. In this study, the FISP was used alone to measure the wound microenvironment, and it was not combined with tissue engineering dressings; thus, this part of the experiment only tested whether the results measured with the FSC were the same as the actual situation. The temperature measured by the FSC at a temperature range from 35 to 42°C (possible temperature range of wounds) in a constant temperature shaker was compared with the recorded temperature, and the mean absolute deviations were profiled (Fig. 2B). The FSC exhibited satisfactory accuracy with a deviation of mostly < 0.3°C (Fig. 2B, red dotted line). The FSC was placed in a constant temperature shaker, and its stability was evaluated by performing continuous readings over 15 min at every two degrees Celsius increase in the range of 33–41°C (possible temperature range of wounds). As shown by the temperature–time curve (Fig. 2C), the temperature sensor displayed a short response time of < 30 s and good long-term stability.

Because the working environment of the system was complicated, the durability of the FSC was evaluated by immersing it in DMEM for different time intervals at 37°C. The FSC worked normally and output a signal when it was immersed in liquid (Fig. S2). No significant change in the measurement deviation was observed within 5 days, but it increased on the 7th day (Fig. 2D), indicating that the FSC had good durability in the normal use time of dressings and could meet the needs of wound monitoring. FSCs are in direct contact with wound tissue and cells, and they should neither be cytotoxic nor negatively affect cell growth. Therefore, we evaluated the cytotoxicity of the FSC and CPCB. L-929 cells were selected as model cells and cocultured with the extraction solution of FSC or CPCB for 1, 3, 5 and

7 days. Cells cultured with DMEM were used as a control. Cell viability was assessed at each time interval using the CCK-8 assay. No significant difference in the absorbance of culture medium between the FSC group and control group, but the absorbance of the CPCB group decreased significantly (Fig. 2E). However, the CPCB was outside the dressings, and thus we showed that the FSC was not cytotoxic during the normal use time of wound dressings. In addition, in a previous study, we also performed systemic acute toxicity tests and skin irritation tests, and the results were satisfactory (Zhang *et al.*, 2020).

Monitoring of the local temperature of wounds infected with different bacteria

We constructed wounds on the rabbit back infected with *S. aureus*, *P. aeruginosa* and *K. pneumoniae* as representative strains to obtain a deeper understanding of the changes in the local temperature of wounds under different bacterial infection states and after debridement dressing changes during wound regeneration and infection. The experimental process is shown in Fig. 3A. Following the operation described above, the FSCs that had been sterilized by soaking in 75% alcohol and ultraviolet irradiation were placed onto the wounds, and four devices were searched simultaneously on the mobile phone through Bluetooth after the devices were turned on (Fig. 3Ba–Bc). After clicking on the device, the corresponding wound information was obtained, and the app received and updated values every 2–10 s (Fig. 3Ca–3Cc). The local temperature information before infection, during infection and after debridement dressing changes were obtained by the FSC and compared with the data from the control group. The changing trend of wound temperature is shown in Fig. 3D. By observing the temperature change curve of the wounds in the control group, we found that the first 3-4 days may be the stage of hyperaemia and inflammation of wound healing in rabbits, and the local temperature increased slightly. As the wounds entered the healing stage, the temperature was in a stable plateau phase. Together with the regeneration process, we decided to apply bacteria to wounds when the wound temperature was stable on the 3rd day after modelling to predominantly eliminate the effect of local temperature changes during the stage of wound hyperaemia and inflammation.

Before infection (days 0 to 3), the local temperature of the wound in each group was approximately 37°C. The wound was inoculated with bacteria on the 3rd day, and the temperature characteristics of different bacteria-infected wounds were explored in the plateau phase of wound temperature. In the infection state (the 4th to 6th days), the local temperature of the wounds infected with
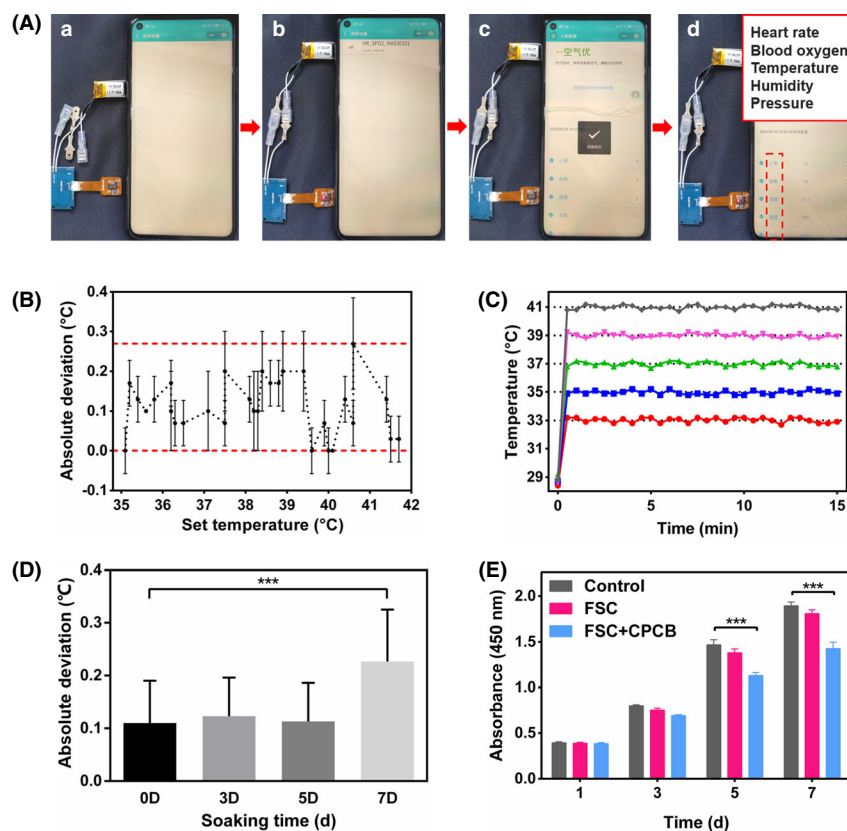
Fig. 2. In vitro operation of the flexible sensing platform and its accuracy, stability, biological durability and biocompatibility.

A. Different working states of the flexible sensing platform in vitro. a. No power supply b. Signal search. c. Connection. d. Display interface (monitoring parameters are shown at higher magnification in the upper right corner).

B. Monitoring accuracy of the temperature sensor in the FISP, which was defined as the deviation between the recorded average temperatures and the corresponding setting temperatures in the range of 33–41°C.

C. Monitoring stability of the temperature sensor in the FISP. This information was profiled by the time-temperature curves that were recorded continuously for 15 min at different temperature settings. D. Durability of the temperature sensor in the sensing module, which was presented as absolute deviation compared with the setting temperature after being soaked in DMEM for different times.

E. Biocompatibility of the sensing module, which was evaluated by measuring the viability of L-929 cells cultured in the extraction solution. Cells cultured in DMEM served as controls ($n = 8$).

S. aureus was approximately 38.5°C, which was the highest among the groups, and the temperatures of wounds infected with *P. aeruginosa* and *K. pneumoniae* were 37.5-38 °C. The average wound temperature of each group on the three days was reported separately (Fig. 3D, right panel). After debridement (after the 6th day), the local temperature of the wounds in the three infection groups gradually decreased to the level of the control. Gram staining of wound samples revealed that cocci were present in the *S. aureus* infection group, and bacilli were present in the other two groups (Fig. S3A). Immunofluorescence staining showed that debridement effectively cleared the biofilm on the surface of wounds, and a small amount of residue was detected in *P. aeruginosa*- and *K. pneumoniae*-infected wounds (Fig. S3B). The results of RT-PCR quantitative analysis of 16S RNA in wound tissue showed that the bacterial load of the wound decreased significantly after debridement

(Fig. S3C). The results of the quantitative analysis of blood agar plate culture of wound exudates showed that the bacterial load of wounds decreased significantly after debridement, and Gram staining of colony smears before debridement identified the corresponding type of bacteria in each group (Fig. 3Ea and Eb). Notably, bacteria were present in wounds of the control group. The bacterial load was $< 10^6$ CFU ml^{-1}, and the result of Gram staining was positive for cocci. Combined with the local temperature change curve of the wound, we found that the wound temperature was related to the type of bacterial infection.

We postulate that the key link leading to the local temperature change was the blood flow in the wound, which was related to inflammatory factors and angiogenesis. Therefore, histological examinations and RT-PCR analyses of wounds were conducted at two time points (5 and 10th days), which represent the infection and after the
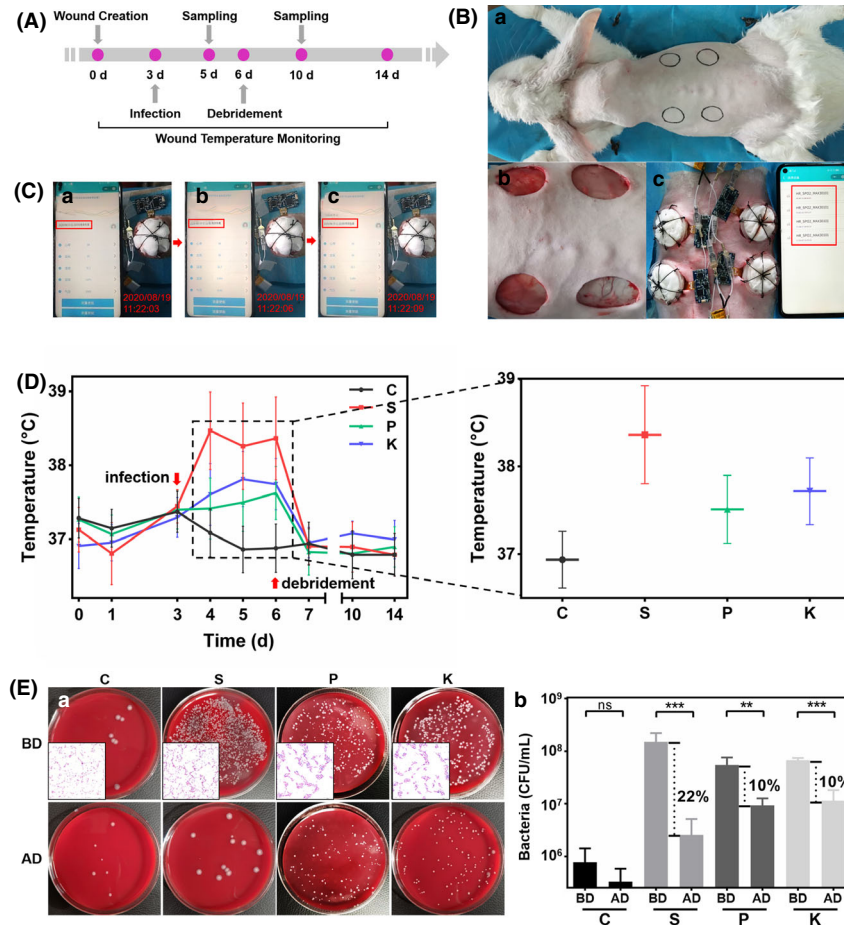
Fig. 3. In vivo study of temperature monitoring in wounds infected with different bacteria.
A. Timeline of the animal experiments.
B. Operational procedure. Four devices can be searched simultaneously on the app interface.
C. Data are updated on the app interface, which receives and uploads data every 2–10 s.
D. Temperature change curve of wounds infected with different bacteria. The high-magnification image on the right shows the local temperature characteristics of the wound under different bacterial infection conditions.
E. a. Blood-agar plate culture of wound exudates before and after debridement and Gram staining of colony smears before debridement. b. Quantitative determination of the bacterial load of wound exudates in different infection groups before and after debridement.

debridement phases, respectively, to reveal the wound status and biological events accompanying the temperature fluctuation. The results of Masson's trichrome staining and RT-PCR showed that the number of inflammatory cells and the expression of inflammatory genes in wounds infected with *S. aureus* were significantly greater than those in other groups, of which the changes were consistent with the wound temperature fluctuations in each group (Fig. S4A, S5A and B). A similar result was observed for wound neovascularization, repair and regeneration (Fig. S4A–S5B). Infection induced the secretion of a large number of inflammatory factors, and the resulting vasodilation was one of the reasons for the increase in the local temperature; the improvement in this condition after debridement also corresponded to the decrease in the local temperature. As

a critical parameter for clinical evaluation, the areas of infected wounds were also analysed (Fig. S5Ca and Cb). The wounds infected with *P. aeruginosa* and *K. pneumoniae* exhibited more serious delayed healing. A series of changes in the wounds from each group was consistent with the corresponding changes in local temperature, which also confirmed the effect of local temperature on indicating wound healing.

Lag of anal temperature indicating wound infection

The 16S RNA FISH staining results of wound samples from each group before and after debridement are shown in Fig. 4A, in which the white dotted line represents the boundary between the dermis and subcutaneous tissue (hereafter referred to as the 'boundary').

On the 2nd day of infection (the 5th day), a large number of bacteria was present in the wounds of each infection group. Bacteria in the *S. aureus* and P. *aeruginosa* infection groups broke through the boundary and invaded deeper, whereas minimal or only trace bacteria were found under the boundary in the *K. pneumoniae* infection group. After debridement (the 10th day), the bacteria on the surface of the wound were basically removed, whereas the deeper bacteria remained. The curve depicting the change in the anal temperature of infected animals is shown in Fig. 4B. On the 1st day after wounds were inoculated with bacteria, the anal temperature of animals in each group did not increase, but that in groups infected with *S. aureus* and *P. aeruginosa* increased on the 2nd day after inoculation. However, the anal temperature of the group infected with *K. pneumoniae* did not increase until the 3rd day. Combined with the results of FISH staining and the local temperature change curve of the wound, we observed a significant lag for the change in anal temperature to show wound infection.

Prediction of wound infection by local temperature

According to the results described above, most of the local temperatures of wounds infected by *P. aeruginosa* and *K. pneumoniae* were concentrated at 37.5–38°C. Considering the difficulty of discrimination in practical applications, we analysed the two combined as representative gram-negative bacteria and *S. aureus* as gram-positive bacteria. All local temperatures of wounds during the infection period were analysed using a multinomial logistic regression analysis (control, gram-positive bacterial infection or gram-negative bacterial infection). The results showed that a higher local wound temperature indicated a greater risk of gram-positive bacterial infection. A lower local wound temperature indicated a lower the risk of infection ($P < 0.001$).

Discussion

A substantial number of cells, cellular factors and trace elements have been proven to participate in the healing process; however, these factors exhibit far less clinical value than previously expected (Sabine and Richard, 2003; Patel et al., 2016). In addition, the disadvantages of traditional clinical experience-based therapy, including infection and medical resource abuse, have been revealed in clinical practice. In the event of large-scale public health events, such as the COVID-19 pandemic, the already inadequate medical resources are unable to meet the regular debridement needs of patients with wounds. The resulting lag in medical interventions is likely responsible for the deterioration of wounds. The

evaluation of clinical outcomes, which guide real-time monitoring and highly effective medical interventions, plays an essential role throughout the treatment of wounds. Four phases comprise the healing process: haemostasis, inflammation, proliferation and tissue remodelling or resolution (Morton and Phillips, 2016). Recent studies have shown that the microenvironment of wounds differs in each stage of healing and under different pathogen infection conditions (Kruse *et al.*, 2015). As a result, we propose a novel method for the visual and dynamic monitoring wound microenvironments using specific sensing components integrated on flexible substrates and combined with biological dressings without disturbing the healing process, providing a promising plan for intelligent wound care.

Although current studies indicate that numerous microenvironmental parameters may share value in predicting wound healing, temperature is particularly worth consideration in regard to clinical practice, given the relatively convincing proof that temperature predicts the clinical outcome of wound beds (Power *et al.*, 2017). However, in our experiment, due to the consistent bandaging method of each experimental group and relatively severe wound exudation, the humidity measured by the sensor chip was always 100%. For systemic indexes, such as heart rate and blood oxygen saturation, we believe that the relationship between these factors and wound healing is uncertain. Thus, the inclusion of all the above factors in the analysis might lead to the cross-effects caused by multiple variables. This study aimed to develop a novel clinical outcome prediction method for use in clinical practice by integrating several technologies, including micro-electronic technology, sensing technology and wireless transmission technology, which are rarely used in the clinical evaluation of wound healing. We imagine the development of a wound microenvironment sensing system where wound-related data would be transmitted from a sensing terminal module to an intelligent module via BLE for real-time clinical monitoring. Then, data would be uploaded to the cloud for further processing and storage through the Internet for remote diagnosis. Continuous monitoring of changes in the wound microenvironment might provide valuable information for clinicians to evaluate clinical efficacy, implement preventive measures in a timely manner and dynamically analyse the risk of infection, which is very important for wound diagnosis and treatment. The wound microenvironment database and the interactive diagnosis and treatment system of wounds based on the LAN platform would be established to realize remote real-time monitoring of the condition of trauma patients between the hospital and communities and to provide basic support for interactive remote expert consultation, diagnosis and nursing. In the future, a wound analysis based on
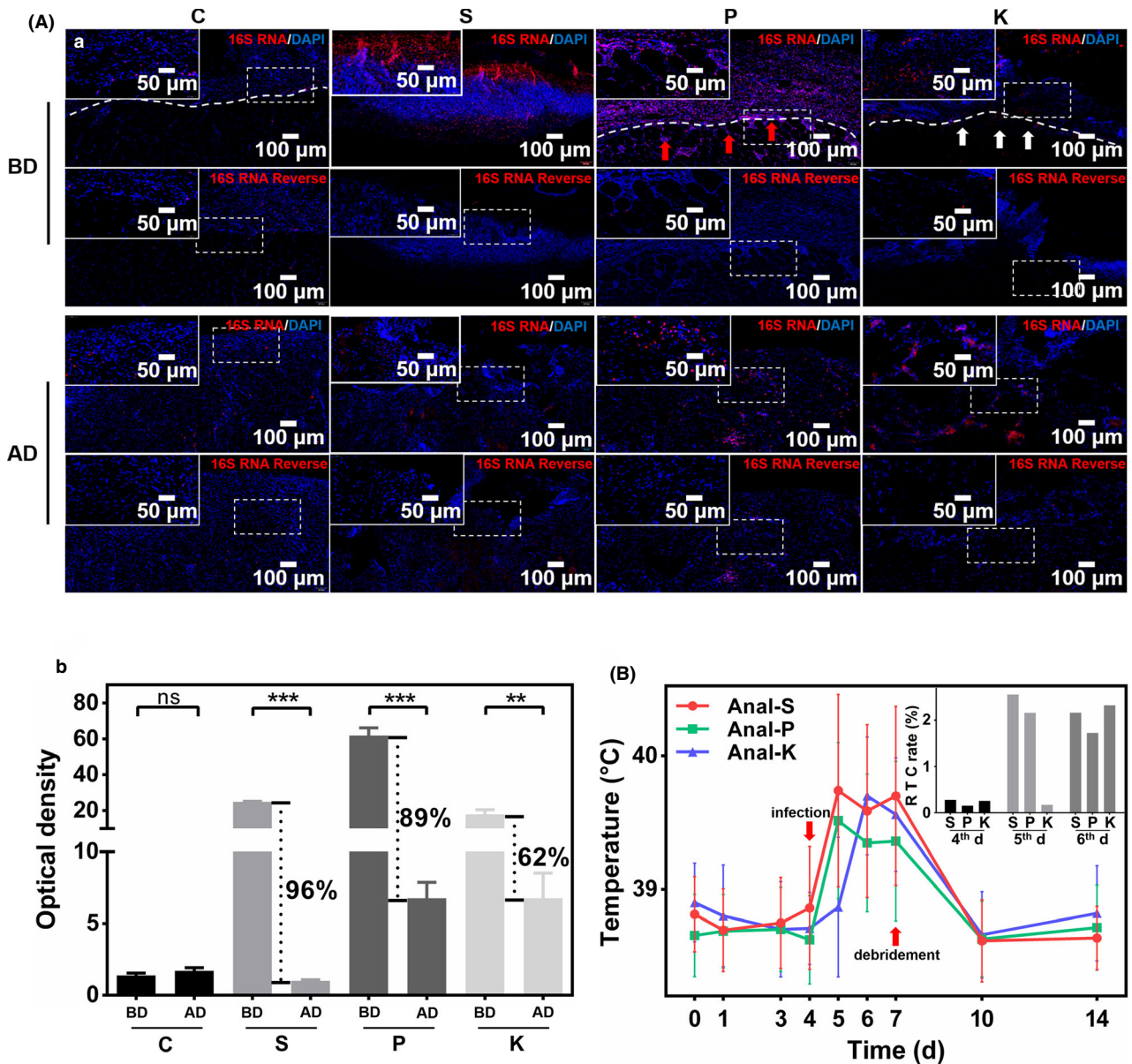
Fig. 4. Bacterial staining of infected wounds and the curve showing the change in the core body temperature of experimental animals.
A. a. 16S RNA FISH staining of each infected wound sample before and after debridement. (The white dotted line represents the boundary between the dermis and subcutaneous tissue. The red arrow indicates the bacteria have broken through the boundary, and the white arrow indicates the bacteria have not broken through that. The upper left corner of each image is the magnified view of the white dotted box. Fluorescence colours: Red, 16S RNA/16S RNA Reverse; Blue, DAPI) b. Quantification of the fluorescence intensity of FISH staining.
B. Curve showing the change in the anal temperature of experimental animals. The graph in the upper right corner presents the time when the anal temperature of each infected group changed significantly.

big data may also provide a new direction for wound treatment.

When designing the wound monitoring system, complex environmental conditions, such as wound temperature and pH range, should be considered. The accurate perception of the wound by the sensor chip is based on good measurement accuracy and stability, which determines whether the measured results truly reflect the

changes in the measured parameters to infer the real-time state of the wound. In our study, the sensing module showed good measurement accuracy, stability and durability. The accuracy of the temperature measurement was no less than that of previous studies (Potyrailo *et al.*, 2011). Qualified equipment should not only meet reasonable stretching requirements during use but also ensure that its function is not affected within a certain

range of stretching (Matsuhisa *et al.*, 2015). The maximum tensile ratio of the FSC was approximately 25%, which was close to the average strain of human skin (Joodaki and Panzer, 2018), and the cyclic tensile test results revealed that the chip had good fatigue resistance. Therefore, we postulated the FSC could withstand normal deformation in the routine use of dressings. The cytotoxicity of the CPCB plate might be caused by the release of metal ions from the solder joint, but it did not come into contact with the wound bed directly and had no effect on the biosafety of smart dressings.

S. aureus, *P. aeruginosa* and *K. pneumoniae* are common pathogens causing infections in our ward. Therefore, we propose that the use of these three pathogens to establish infected wounds is representative to some extent. As the inflammatory response after injury induces an increase in wound temperature (Power *et al.*, 2017), methods to distinguish an early infection from injury-induced inflammation should be considered. Therefore, we chose to inoculate the wound with bacteria on the third day after the wound temperature was stable to balance the effect of inflammation on local temperature after injury. In addition, the establishment of a control group and an infection group in the same animal also excluded the possible effect of the increase in body temperature caused by infection on the local temperature of wounds. The changes in the wound microenvironment caused by different bacterial infections are bound to be different. On the one hand, infection leads to the secretion of various inflammatory factors, resulting in vasodilation. On the other hand, infection may stimulate the angiogenesis of the wound through a feedback mechanism, thus increasing the blood flow to clear the infection as soon as possible. All these factors explain the increase in the local temperature of the infected wound. In our experiment, the temperature of wounds infected with *S. aureus* was significantly increased compared with wounds infected with the other two species. This finding is consistent with the 'positive' and 'negative' infection symptoms of gram-positive bacteria and gram-negative bacteria, which may be related to the exotoxins secreted by *S. aureus*. On the first day after inoculation of bacteria in the wound, we observed a significant increase in the local temperature of the wound, whereas the increase in anal temperature in animals was delayed to the 2nd or 3rd day. The increase in anal temperature in experimental animals exhibited a lag, which may be attributed to the amount of time required for bacteria to break through the boundary into the blood. Moreover, the difference in invasiveness of different bacterial strains explains the difference in the time of breaking through the boundary, as indicated by the anal temperature.

Microbial colonization of the wound is inevitable, and endogenous bacteria are dominant. When the bacterial load exceeds the host defences, infection will occur (Robson *et al.*, 1999). The level of bacteria that is tolerated for normal healing without the possibility for invasive infection appears to be 10^5 bacteria per gram of tissue for all species studied (Heggers and Robson, 1990). When a critical number of bacteria greater than this level are present, the tissue responds with an infection (Robson *et al.*, 1999). When locally colonized bacteria form biofilms, they prevent antibiotic infiltration, escape from innate immune attacks by phagocytes and consequently generate bacterial resistance (Zhang *et al.*, 2020). As a traditional treatment, debridement and dressing changes remove most bacteria, biofilms, virulence factors and necrotic tissue (Daeschlein, 2013). However, the process does not seek to make the wound aseptic but to return it to a state of bacterial balance to embark upon the correct healing track. Due to the high body temperature, the wounds of rabbits are less susceptible to infection. We used a large amount of a single strain to ensure the colonization of bacteria and the spread of local infection in this radical modelling method. Therefore, the corresponding changes in the wound microenvironment should be caused by the infection of the bacteria used here. In animal experiments, the consistency of modelling methods, wound bacterial load and infection time will inevitably lead to the consistency of changes in the wound microenvironment. However, in clinical practice, the wound condition is not as simple as that noted in animal experiments, as a variety of mixed bacterial infections might occur (Abrahamian and Goldstein, 2011; Libertucci et al., 2019). In this case, a large amount of wound microenvironment information must be collected and combined with the bacterial culture results to establish the wound microenvironment database. The bacteria that cause changes in the wound microenvironment were matched and screened through a high-throughput analysis to provide some insights into the actual clinical situation.

In the process of diagnosis and treatment, clinicians are often at a loss when attempting to determine the treatment of 'unknown' wounds wrapped in dressings, and the 'unknown' state also leads to the use of only extended-spectrum antibiotics or even a combination of antibiotics to treat or even prevent the occurrence of infection before the aetiological results are reported, although this approach does not meet the diagnostic and treatment standards (Jones and Samore, 2017). To some extent, this method has led to more rampant drug-resistant bacteria; for example, the more common infectious bacteria identified in the burn ward have shifted to MRSA and *P. aeruginosa* with strong drug resistance (Rezaei *et al.*, 2011; Lachiewicz *et al.*, 2017; D'Abbondanza and Shahrokhi, 2020). The emergence of the FISP might slightly improve this vicious circle. Of course,

the judgement of the wound state based on the microenvironment cannot replace the gold standard of an aetiological diagnosis, and the identification of the pathogen causing a wound infection based on a single index of local temperature is arbitrary and impractical. However, at least during the 'window period' before the aetiological results are reported, clinicians could make a preliminary judgement on the basic condition of the wound, i.e., whether an infection is present. According to our results, the local temperature of the wounds infected with *P. aeruginosa* and *K. pneumoniae* was approximately 37.5–38°C, and the changes in histology and expression of various genes were basically consistent. These results are quite different from those of the wounds infected by *S. aureus*. This finding indicates that the local temperature of wounds exerts a specific effect on the pathogen causing the wound infection. Therefore, clinicians could choose antibiotics purposefully, which may contribute to alleviating the abuse of antibiotics and reducing the emergence of drug-resistant bacteria.

The use of the FISP to visualize the wound microenvironment is more convenient for clinicians to evaluate the state of wound healing and make correct treatment decisions. Abundant microenvironmental parameters can indicate the state of the wound and are thus helpful tools for the non-invasive monitoring and early detection of non-healing wounds or infections (Kruse *et al.*, 2015). In addition to temperature, several parameters, including local pH, glucose, lactic acid, and uric acid, might represent available candidates for subsequent research. We propose that the richer the microenvironment index, the more accurate the estimate of the state of the wound. Furthermore, we anticipate the day that the wound microenvironment monitoring system would become strengthened and further developed through the increased richness of monitoring indicators, the wound clinical outcome algorithm, more intelligent medical treatment programmes for casualties and the analysis of data for the distribution and severity of acute or chronic wounds. We postulate that intelligent and individual wound care and diagnosis based on the wide application of 'big data' and the Internet of Things represents the future of clinical wound management.

Conclusions

In this study, we constructed a FISP to monitor the local temperature of wounds and other physiological parameters in real time, and a customized app installed on a smartphone was applied for data exchange and display. The device was designed as a separate structure composed of an FSC and CPCB. The FSC was in direct contact with the wound and was combined with a variety of functional dressings. The CPCB was outside the dressing and used for processing and transmitting sensor information. The equipment exhibited good skin compliance, measurement accuracy, stability, biological durability and biocompatibility. We applied this system to infected wounds on the rabbit back to verify that the device could monitor the wound local temperature in real time and reveal the changes based on different bacterial infection conditions, potentially prompting the identification of the pathogen causing the wound infection to some extent. We believe that with the further development of our work and the inclusion of other local indicators, such as local pH, uric acid, lactic acid and glucose, the FISP will play an important role in precision medicine, telemedicine and AI diagnosis and is expected to lead to the development of a new wound management model.

Experimental procedures

Fabrication of the FISP

The FISP consisted of an FSC and a CPCB. Connected to the CPCB through a flexible flat cable (FFC), the FSC was processed with a 35-μm-thick copper film using 25 μm polyimide (PI) as the substrate. Temperature and humidity sensors (HTU21D, Humirel, France) and other components were welded (Li *et al.*, 2020). The CPCB included a BLE antenna (Rainsun, Taiwan, China), digital controller (NRF51822; Nordic, Trondheim, Norway) and power management (TP4056; NanJing Top Power ASIC Corp, Nanjing, China). Before usage, the FSC was encapsulated within a thin polydimethylsiloxane (PDMS) layer to ensure that the system had good tightness and biocompatibility.

Skin compliance assay

The tensile properties of the substrate of the FSC were determined using an electronic universal testing machine (CMT 5304; Shenzhen Sansi, Shenzhen, China). The substrate sample with a gauge length of 30 mm and a width of 7 mm was tested at room temperature with a stretch rate of 5 mm min^{-1}. Young's modulus was calculated from the slope of the stress–strain curve. Cyclic tensile tests were also performed by sequential loading and unloading at a rate of 10 mm min^{-1} for 20 cycles with a maximum strain of 7% using an electronic universal testing machine (UTM 2203; Jinan Kesheng, Jinan, China).

Accuracy and stability tests

The sensor testing method was carried out as described in a previous study (Lou *et al.*, 2020). Briefly, the sensor chip was placed in a constant temperature shaker (LYZ-

100B; Longyue, Shanghai, China), and the temperature was gradually increased. One hundred pairs of data were obtained at the same time in the range of 33–41°C, and 30 pairs of data were randomly selected for analysis. In addition, the stability was tested by placing the sensor chip in an incubator (Thermo Fisher Forma 371; Thermo, Waltham, MA, USA) with temperature settings of 33, 35, 37, 39, and 41°C for 15 min, separately, and the data were recorded every 30 s. All the experiments were repeated thrice.

Durability and cytotoxicity tests

The sensor chip was immersed in Dulbecco's modified Eagle's medium (DMEM; HyClone, Los Angeles, CA, USA) at 37°C for 3, 5, and 7 days to simulate the humid and liquid wound environment in vivo. At each time point, the sensor chip was directly powered and 30 sets of temperature data were recorded. The cytotoxicity of the integrated device was evaluated by determining the viability of L-929 cells cultured with the extraction medium. Briefly, the FSC was soaked in DMEM at 37°C for 24 h at a concentration of 1 cm^2 ml^{-1} (area of device/volume of DMEM) to collect the extraction solution. Cells were seeded in a 96-cell plate at a density of 1×10^4 cells ml^{-1} and cultured with the extraction solution for 2, 4 and 7 days. Cells cultured in pure DMEM were used as a control. At each time interval, CCK-8 (7seabiotech, Shanghai, China) was added to the culture system and incubated for 3 h at 37°C. Subsequently, cell viability was evaluated by determining the absorbance at 500 nm using a microplate reader (Model 200 PRO; Tecan, USA). All the experiments were repeated thrice.

Establishment, treatment and monitoring of the wound model

Animal experiments were performed in accordance with protocols approved by the Ethics Committee of Tangdu Hospital. New Zealand rabbits (4–5 kg, female, obtained from Experimental Animal Centre of Fourth Military Medical University, Xi'an, China) were acclimated for 2 weeks before the experiments. Fifty-one animals were used in this study. All animals were anaesthetized by an intravenous injection with pentobarbital sodium (30 mg kg^{-1}) before the surgical procedure. The area was disinfected with a povidone-iodine solution and then with 75% ethyl alcohol after the hair was shaved. Four standardized 3.5 cm diameter full-thickness wounds were created between the crest of the shoulders and the coccygeal tuberosity on either side of the back at 1.5 cm on each side of the median line of the dorsal spine. The wounds were fixed with circular plastic moulds to prevent contraction. Each wound was created with an area of

approximately 9.6 cm^2, and the total wound area was < 10% of the animal's total body surface area. All procedures were performed by the same surgeon. The surfaces of all wounds were placed on a flexible sensor platform and packed with gauze. All experimental animals were randomly divided into the *Staphylococcus aureus* infection group ($n = 17$, ATCC29213), *Pseudomonas aeruginosa* infection group ($n = 17$, ATCC27853) and *Klebsiella pneumoniae* infection group ($n = 17$, ATCC4352). A bacterial suspension (5 mL) with an initial density of 10^8 CFU ml^{-1} was prepared and inoculated into two wounds on the right side of the back of the specified group on the 3rd day after modelling, and the contralateral side was treated with the same amount of normal saline. Then, the wounds were covered as described above. Routine debridement was performed on the 6th day. The wound temperature was continuously monitored after modelling, and the values were recorded at 0, 1, 3, 4, 5, 6, 7, 10 and 14 days at the same time of day. At the same time, the anal temperature was measured with a mercury thermometer. The wound temperature recorded at 12 h after the operation was designated day 0 to eliminate the effect of anaesthesia on the wound temperature of animals. All data were collected before wound treatment on the same day, and the temperature of wounds collected was not included in the analysis.

Detection of bacteria in the wound exudate

Before and after debridement (on the 5 and 10th days), 1 μl of wound exudate was diluted to 10 ml in each group, and 100 μL of the exudate were smeared on a blood agar plate and incubated at 37°C for 24 h. The number of colonies was quantified using ImageJ software, and the bacterial concentration of the corresponding wound exudate was calculated. The colony smears before debridement were subjected to Gram staining (ZHHC, Xi' an, China).

Histological examination

The wound specimens obtained at each time point from each group were divided into three parts and treated properly. Two of the portions were fixed with 4% paraformaldehyde or a FISH special fixative liquid at 4°C overnight, dehydrated with a graded series of ethanol solutions and embedded in paraffin. After continuous slicing, follow-up experiments were performed. Wound bacteria and biofilms are shown in the images of FISH and immunofluorescence staining respectively. Masson's trichrome staining and immunohistochemical staining were used to evaluate the wound status and angiogenesis. All sections were observed and photographed with

an optical microscope (IX73; Olympus, Tokyo, Japan), and ImageJ software was used to analyse all images.

Immunohistochemical and immunofluorescence staining

Sections were first deparaffinized and rehydrated, and then antigen retrieval was performed by incubating slides in a Pepsin solution (7seabiotech) for 20 min at 37 °C. Samples were stained with a rabbit anti-rabbit VWF antibody (Bioss, Beijing, China) and subsequently stained with anti-rabbit IgG. HRP-streptavidin was then added, followed by the incubation of sections with the AEC substrate (Solarbio, Beijing, China) to reveal the staining. After antigen retrieval, the sections were treated with Con A 647 (1:1000; Invitrogen, Waltham, MA, USA) in a dark room for 20 min, washed thoroughly and incubated with DAPI (1:1000; 7 Seabiotech) for 15 min. After rinsing, the sections were sealed with glycerol and observed.

FISH staining

After antigen retrieval, sections were dehydrated and air-dried, followed by denaturation for 10 min at 75°C and the hybridization of 4 ng μl^{-1} probes for 16 h at 37°C in FISH hybridization buffer (7seabiotech). Oligonucleotide probes (EUB338: 5'-GCTGCCTCCCGTAGGAGT-3') targeting 16S RNA of most bacteria labelled with Cy3 were used, and labelled probes designed with the reverse sequence of EUB338 were used as controls. Slides were then washed with post-hybridization wash buffer (7seabiotech), incubated with DAPI (7seabiotech) for 15 min, and analysed using a Nikon A1R SI confocal microscope.

RT-PCR analysis

Total RNA was extracted from bacterial and host-derived DNA in frozen specimens with the UNIQ-10 Column TRIzol Total RNA Isolation Kit (Sangon Biotech, Shanghai, China) according to the manufacturer's protocol. The concentration of total RNA was determined using BioPhotometer Plus (Eppendorf, Hamburg, Germany), and reverse transcription reactions were performed with 100 ng of total RNA using PrimeScript™ RT Master Mix (TaKaRa, Shiga Prefecture, Japan). Real-time PCR was conducted using the SYBR Green system with the primer sets shown in Table S1. Real-time PCR was performed using the CFX Connect Real-Time system (Bio-Rad, CA, USA) at 95°C for 10 min and 40 cycles of amplification consisting of a denaturation step at 95°C for 15 s and an extension step at 60°C for 1 min. The gene expression level, which was normalized to GAPDH, was then calculated using the 2-ΔΔt formula. Data are presented as $1/C_t$ values. The relative proportion of 16S vs. 18S RNA was used to calculate the absolute quantities of bacterial and host-derived DNA. The primers are listed in Table S1.

Statistical analysis

SPSS 19.0 software was used for statistical analyses. Values are presented as the means and standard deviations, and pair-wise comparisons were performed using t-tests, paired t-tests and one-way ANOVA. The Bonferroni method was used for comparisons between groups. The prediction models of wound infection were established using the disordered multiclassification logistic regression method. At the test level $n = 0.05$, $P < 0.05$ indicates that the difference is statistically significant, $*P < 0.05$, $**P < 0.01$, and $***P < 0.001$.

Conflict of interests

The authors have no competing interests to declare.

References

Abrahamian, F.M., and Goldstein, E.J. (2011) Microbiology of animal bite wound infections. *Clin Microbiol Rev* **24:** 231–246.

Collier, M., and Hollinworth, H. (2000) Pain and tissue trauma during dressing change. *Nurs Stand* **14:** 71–73.

D'Abbondanza, J.A., and Shahrokhi, S. (2020) *Burn Infection and Burn Sepsis, Surg Infect (Larchmt).*

Daeschlein, G. (2013) Antimicrobial and antiseptic strategies in wound management. *Int Wound J* **10(Suppl** 1): 9–14.

Fierheller, M., and Sibbald, R.G. (2010) A Clinical investigation into the relationship between increased periwound skin temperature and local wound infection in patients with chronic leg ulcers. *ADV Skin Wound Care* **23:** 369–379.

Frykberg, R.G., and Banks, J. (2015) Challenges in the treatment of chronic wounds. *Adv Wound Care (New Rochelle)* **4:** 560–582.

Heggers, J.P., and Robson, M.C. (1990) *Quantitative Bacteriology: Its Role in the Armamentarium of the Surgeon.* Boca Raton, FL: CRC Press.

Jones, B.E., and Samore, M.H. (2017) Antibiotic overuse: clinicians are the solution. *Ann Intern Med* **166:** 844–845.

Joodaki, H., and Panzer, M.B. (2018) Skin mechanical properties and modeling: a review. *Proc Inst Mech Eng H* **232:** 323–343.

Junker, J.P., Caterson, E.J., and Eriksson, E. (2013) The microenvironment of wound healing. *J Craniofac Surg* **24:** 12–16.

Kruse, C.R., Nuutila, K., Lee, C.C.Y., Kiwanuka, E., Singh, M., Caterson, E.J., *et al.* (2015) The external microenvironment of healing skin wounds. *Wound Repair Regen* **23:** 456–464.

Kurz, A., Sessler, D.I., and Lenhardt, R. (1996) Perioperative normothermia to reduce the incidence of surgical-wound infection and shorten hospitalization. *N Engl J Med* **334:** 1209–1215.

Lachiewicz, A.M., Hauck, C.G., Weber, D.J., Cairns, B.A., and van Duin, D. (2017) Bacterial infections after burn injuries: impact of multidrug resistance. *Clin Infect Dis* **65:** 2130–2136.

Li, Y., Mao, Y., Xiao, C., Xu, X., and Li, X. (2020) Flexible pH sensor based on a conductive PANI membrane for pH monitoring. *RSC Adv* **10:** 21–28.

Libertucci, J., Bassis, C. M., Cassone, M., Gibson, K., Lansing, B., Mody, L., et al. (2019) Bacteria detected in both urine and open wounds in nursing home residents: a pilot study. *mSphere* **4:** e00463-19.

Lindholm, C., and Searle, R. (2016) Wound management for the 21st century: combining effectiveness and efficiency. *Int Wound J* **13:** 5–15.

Lou, D., Pang, Q., Pei, X., Dong, S., Li, S., Tan, W.-Q., and Ma, L. (2020) Flexible wound healing system for pro-re-generation, temperature monitoring and infection early warning. *Biosens Bioelectron* **162:** 112275.

Marieke, H. (2018) Chronic wounds innovations in diagnostics and therapeutics. *Curr Med Chem* **25:** 5772–5781.

Matsuhisa, N., Kaltenbrunner, M., Yokota, T., Jinno, H., Kuribara, K., Sekitani, T., and Someya, T. (2015) Printable elastic conductors with a high conductivity for electronic textile applications. *Nat Commun* **6:** 7461.

Matzeu, G., Fay, C., Vaillant, A., Coyle, S., and Diamond, D. (2016) A wearable device for monitoring sweat rates via image analysis. *IEEE Trans Biomed Eng* **63:** 1672–1680.

McGuiness, W., Vella, E., and Harrison, D. (2004) Influence of dressing changes on wound temperature. *J Wound Care* **13:** 383–385.

Morton, L.M., and Phillips, T.J. (2016) Wound healing and treating wounds: differential diagnosis and evaluation of chronic wounds. *J Am Acad Dermatol* **74:** 589–605; quiz 605–586.

Nicholas, A.R., Andrea, D.M., and Alejandra, C.V. (2013) Evidence-based management of common chronic lower extremity ulcers. *Dermatol Ther* **26:** 187–196.

Olsson, M., Jarbrink, K., Divakar, U., Bajpai, R., Upton, Z., Schmidtchen, A., and Car, J. (2019) The humanistic and economic burden of chronic wounds: a systematic review. *Wound Repair Regen* **27:** 114–125.

Pang, Q., Lou, D., Li, S., Wang, G., Qiao, B., Dong, S., *et al.* (2020) Smart flexible electronics-integrated wound dressing for real-time monitoring and on-demand treatment of infected wounds. *Adv Sci (Weinh)* **7:** 1902673.

Patel, S., Maheshwari, A., and Chandra, A. (2016) Biomarkers for wound healing and their evaluation. *J Wound Care* **25:** 46-55.

Payam, Z., Abolfazl, S. M., Saeed, M., Zhaleh, A., Anahita, A., Mohammad, A. A., et al. (2017) Can regenerative medicine and nanotechnology combine to heal wounds? The search for the ideal wound dressing. *Nanomedicine* (Lond.) **12:** 2403–2422.

Phillips, C.J., Humphreys, I., Fletcher, J., Harding, K., Chamberlain, G., and Macey, S. (2016) Estimating the costs associated with the management of patients with chronic wounds using linked routine data. *Int Wound J* **13:** 1193–1197.

Potyrailo, R.A., Wortley, T., Surman, C., Monk, D., Morris, W.G., Vincent, M., *et al.* (2011) Passive multivariable temperature and conductivity RFID sensors for single-use biopharmaceutical manufacturing components. *Biotechnol Prog* **27:** 875–884.

Power, G., Moore, Z., and O'Connor, T. (2017) Measurement of pH, exudate composition and temperature in wound healing: a systematic review. *J Wound Care* **26:** 381–397.

Powers, J.G., Higham, C., Broussard, K., and Phillips, T.J. (2016) Wound healing and treating wounds: chronic wound care and management. *J Am Acad Dermatol* **74:** 607–625; quiz 625–606.

Rezaei, E., Safari, H., Naderinasab, M., and Aliakbarian, H. (2011) Common pathogens in burn wound and changes in their drug sensitivity. *Burns* **37:** 805–807.

Robert, G.W., and Martin, U. (2012) Wound cleaning and wound healing: a concise review. *Adv Skin Wound Care* **26:** 160–163.

Robson, M.C., Mannari, R.J., Smith, P.D., and Payne, W.G. (1999) Maintenance of wound bacterial balance. *Am J Surg* **178:** 399–402.

Ruth, E.J., Deshka, S.F., and Michael, T.L. (2018) Management of chronic wounds-2018. *JAMA* **320:** 1481–1482.

Sabine, W., and Richard, G. (2003) Regulation of wound healing by growth factors and cytokines. *Physiol Rev* **83:** 835–870.

Sen, C.K., Gordillo, G.M., Roy, S., Kirsner, R., Lambert, L., Hunt, T.K., *et al.* (2009) Human skin wounds: a major and snowballing threat to public health and the economy. *Wound Repair Regen* **17:** 763–771.

Tegl, G., Schiffer, D., Sigl, E., Heinzle, A., and Guebitz, G.M. (2015) Biomarkers for infection: enzymes, microbes, and metabolites. *Appl Microbiol Biotechnol* **99:** 4595–4614.

Zhang, Y.H., Han, B., Pan, Z.P., Zhang, C., Xu, X.L., and Li, X.Y. (2020) Development and characteristic evaluation of wireless sensor module for wound temperature and pressure. *Chin J Burns* **36:** 671–678.

Zhang, Y., Pi, Y., Hua, Y., Xie, J., Wang, C., Guo, K., *et al.* (2020) Bacteria responsive polyoxometalates nanocluster strategy to regulate biofilm microenvironments for enhanced synergetic antibiofilm activity and wound healing. *Theranostics* **10:** 10031–10045.

Supporting information

Additional supporting information may be found online in the Supporting Information section at the end of the article.

Fig. S1. Various applications of the FISP. A. Telemedicine, AT diagnosis, and precision medicine. B. In peacetime, it could be used to provide community medical care and conveniently employed for remote guidance for doctors. C. In the event of public health events, such as COVID-19, it could be used for centralized monitoring of ward patients' wounds to save scarce medical resources.

Fig. S2. A. The FISP immersed in liquid still operates in a stable manner.

Fig. S3. A. Gram staining of wound tissue before and after debridement. B. Immunofluorescence staining of wounds before and after debridement in each group (Red: Con A 647; Blue: DAPI). C. RT-PCR quantification of bacterial 16S RNA in the wound tissue from each infection group before and after debridement. (a-d: Control, *S. aureus*-infected, *P. aeruginosa*-infected and *K. pneumoniae*-infected groups, respectively).

Fig. S4. Masson and immunohistochemical staining of wounds in each group. A. Masson staining of wounds in each group before and after debridement. B. Quantitative analysis of vessel number (a) and vascular area (b) before and after debridement. C. VWF immunohistochemical staining of wounds before and after debridement in each group.

Fig. S5. Photos of infected wounds and expression of genes related to inflammation, neovascularization, repair and regeneration. A. Expression heat map of various genes. B. Quantitative analysis of various genes. C. a. The healing process of each infected wound. b. The change of wound area.

Table S1. RT-PCR Primer.